Copper Nanowires as Nanoscale Interconnects: Their Stability, Electrical Transport, and Mechanical Properties

Wei-Hong Xu, Lei Wang, Zheng Guo, Xing Chen, Jinhuai Liu, and Xing-Jiu Huang*

Research Center for Biomimetic Functional Matreials and Sensing Devices, Institute of Intelligent Machines, Chinese Academy of Sciences, Hefei, Anhui 230031, PR China

ABSTRACT Application of copper nanowires (Cu NWs) for interconnects in future nanodevices must meet the following needs: environmental stability and superior electrical transport properties. Here, we demonstrate a kind of Cu NW that possesses the both properties. The Cu NWs were synthesized through a hydrothermal route with the reduction of copper chloride using octadecylamine (ODA). The reasons for their environmental stability could be due to interaction of ODA^+ molecules with the surface of Cu NWs and forming strong N—Cu chemical bonds. Electrical transport properties of individual Cu NW were investigated by using the four-probe measurement, showing the temperature-dependent resistance of the Cu NW was fairly linear in the temperature range from 25 to 300 K and the Cu NW retained the low resistivity of approximately $3.5 \times 10^{-6}\ \Omega \cdot cm$ at room temperature, near the resistivity value of bulk copper. The maximum transport current density for the Cu NW should be superior to $1.06 \times 10^7\ A \cdot cm^{-2}$. In addition, the Cu NWs have ultralow junction resistance. The present study indicates that the Cu NWs could act as a multifunctional building blocks for interconnects in future nanoscale devices.

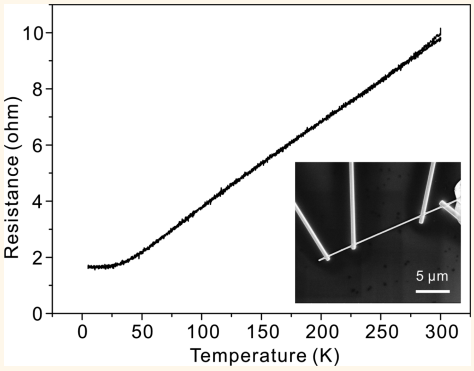

KEYWORDS: Cu NWs · environmental stability · mechanical properties · electrical transport properties · interconnects · nanoscale devices

Future integrated chips might change from a planar array to a vertical configuration in order to increase the device density.[1] Interconnects are an essential part of these architectures, which provide the electrical paths needed in a circuit to pass signals and data between different functional blocks.[2] Suitable nanowires (NWs) for interconnects, precise positioning of NWs and welding at the nanoscale are key issues. Recently, latest innovative development in nanomanipulation and assembly,[3−5] as well as nanowire bonding techniques,[6,7] demonstrates the future feasibility of practical use of conductive NWs in nanoelectronic devices as interconnects.

The NWs for interconnects should be of long-term stability and superior electrical transport properties because NWs with great resistance will result in power loss, signal degradation, and other performance limitations.[8,9] Many kinds of one-dimensional (1D) conductive nanomaterials have been intensively exploited in the past few years, such as carbon nanotubes (CNTs),[10] metal NWs (*e.g.*, Ag,[11−16] Au,[8,9] Cu,[17−20] Mo,[21] Pb,[22,23] Pt,[24] *etc.*), inorganic compound NWs (*e.g.*, RuO_2,[25] Ni_3Si,[26] *etc.*), and organic compound NWs (*e.g.*, polyindole,[27] tetraaniline,[28] *etc.*). 1D conductive organic and inorganic compound NWs usually possess low conductivity, need doping to tune their electrical properties, and remain a challenge in size and shape control compared with their metal counterparts.[25−28] Metallic CNTs are a kind of ideal candidate for interconnects, but the difficulty in controlled synthesis of clean metallic CNTs limited their broad applications because their semiconducting or metallic features are strongly dependent on their diameter and chirality.[29−32]

Among the metals, Au, Ag, and Cu all show high electrical conductivity. Kotov and coworkers have shown that the 92 and 185 nm

* Address correspondence to xingjiuhuang@iim.ac.cn.

Received for review July 24, 2014 and accepted December 18, 2014.

Published online December 18, 2014
10.1021/nn506583e

© 2014 American Chemical Society

diameter Au NWs can possess near-bulk conductivity if the NWs are highly crystalline and are highly smooth.[9] We have reported that the core/shell nanocables of Ag@C are very stable, and the Ag NW core can almost retain the conductivity of bulk silver.[14] The excellent electrical transport properties of Au and Ag NWs make them an ideal candidate as interconnects for linking nanoscale devices, but copper is more abundant and less expensive than gold or silver and is currently widely used in different commercial ways. The study of intrinsic electrical properties of individual Cu NWs in the past faced some challenges, including easy oxidation, low aspect ratio, and polycrystallinity.[17−20,33,34] Recently, we extended the core/shell nanostructure of Ag@C to cupreous congeners and also found that Cu NW core keeps the excellent properties of the bulk counterpart.[35] Additionally, Schimmel and co-workers investigated the 400 nm diameter highly twinned Cu NWs to remain near-bulk conductivity of the bulk copper.[17] But these novel nanostructures were difficult to be controllably synthesized and purified. Thus, facile synthesis of single-crystalline Cu NWs with large aspect ratio, environmental stability, and excellent electrical properties is of great significance in both material science and nanotechnology.

Simultaneously, if Cu NWs have real applications as interconnects and active components of nanoelectronic devices, the reliability and functionality of those nanodevices would depend on their mechanical properties.[36] However, few reports are available on their mechanical properties. Such studies are important because Cu NWs may be subjected to mechanical or electrical stress during device processing or operation, and such stresses may affect the properties of the nanowires.[37]

Herein, we demonstrate a facile hydrothermal route with the reduction of copper chloride using octadecylamine (ODA) to fabricate Cu NWs that show stable in air for more than a year, and a type of nanodevice constructed from individual Cu NW was fabricated by using a focused-ion-beam (FIB) deposition technique. A four-probe measurement was applied to investigate the electrical transport properties of individual Cu NW, showing that the temperature-dependent resistance of the Cu NW was fairly linear in the temperature range from 25 to 300 K and the Cu NW retained low resistivity of approximately $3.5 \times 10^{-6}\ \Omega\cdot$cm, in the same order as that of bulk copper ($1.723 \times 10^{-6}\ \Omega\cdot$cm), and the Cu NWs exhibited the size-dependence of the mechanical strength.

RESULTS AND DISCUSSION

Structural and Morphological Characterization. The morphology and dimensions of the as-prepared Cu NWs were examined by scanning electron microscopy (SEM). Parts a−c of Figure 1 show clean, ultralong, and flexible Cu NWs on a large scale that could be routinely achieved using this synthetic approach. Most of NWs are 50−300 nm in diameter. The inset in Figure 1a is the photograph of the as-prepared red textile-like Cu nanowire networks, which consist of copious Cu NWs being spontaneously woven together during the hydrothermal process. Optical images of the Cu NW networks also show the clean and continuous structures of the Cu NWs, demonstrating that the nanowires are even up to several centimeters in length (see the Supporting Information, Figure S1), resulting in an aspect ratio of about 10^5−10^6. Figure 1d shows a TEM image of an individual Cu NW of about 50 nm in diameter that is uniformly covered with an adsorbate layer with a

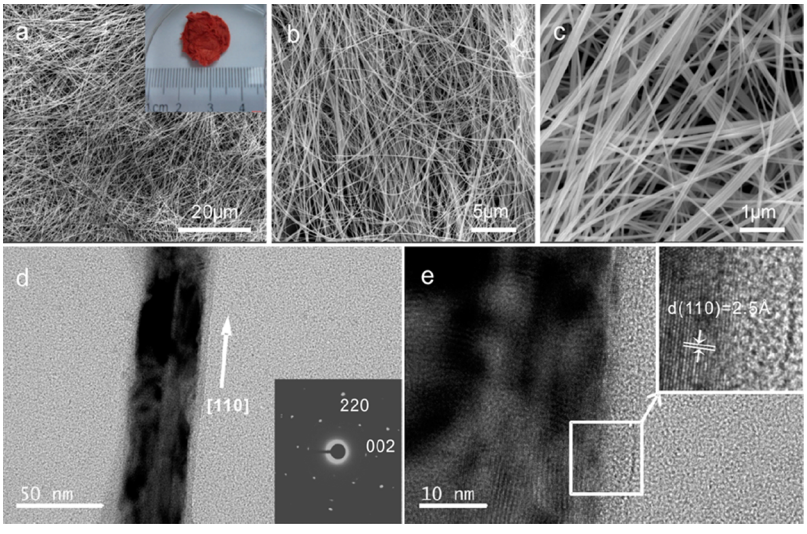

Figure 1. (a−c) SEM images of Cu nanowires at different magnifications, showing clean and uniform Cu nanowires with a diameter of 50−300 nm. The inset in (a) is the photograph of the as-prepared red textile-like Cu nanowire networks, indicating that the nanostructures even grow up to several centimeters in length. (d) TEM image of an individual Cu nanowire of about 50 nm in diameter, showing an adsorbate layer (3−4 nm in thickness) on the surface of the Cu nanowire. The inset is the corresponding SAED pattern. (e) HRTEM image of the Cu nanowire shown in (d). The inset is a local enlarged view of the boxed region.

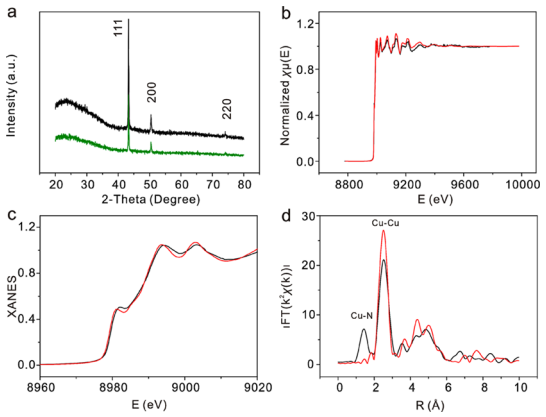

Figure 2. (a) XRD pattern of the as-prepared Cu nanowires (olive line) and the same sample (black line) stored in ambient atmosphere after more than a year, (b) normalized XAFS spectrum at Cu *K*-edge, (c) normalized Cu *K*-edge XANES, and (d) radial distribution function after Fourier transform of EXAFS spectra of Cu foil (red line) and Cu NW sample (black line) under synchrotron X-ray irradiation, respectively.

thickness of about 3−4 nm. Further fine structure of the Cu NW was then characterized by HRTEM, as shown in Figure 1e. The inset of Figure 1e demonstrates a local enlarged HRTEM image from the boxed region, clearly seeing the interface between the crystalline Cu NW and the apparent nonstructured amorphous adsorbate layer. HRTEM image of the single Cu NW displays the lattice fringe distances are about 2.5 Å, corresponding to Cu(110) interplanar spacing, which indicates that the Cu NWs are well crystallized along the [110] growth direction, in good agreement with an analysis by selected-area electron diffraction (SAED) pattern (inset of Figure 1d). The thin adsorbate layer could be made up of the protonized ODA^+ which adsorbed onto the surface of Cu NW during the reaction process of ODA reducing copper(II) to metallic copper.[19] This hypothesis can be further proved *via* the FTIR spectrum of the obtained nanowires compared with that of pure ODA (see the Supporting Information, Figure S2). There is a strong absorption peak shifting from 3336 to 3446 cm^{-1}, which can be assigned as the absorption peak of $\upsilon_{NH_3^+}$ of the protonized ODA^+. The growth mechanism of the as-prepared Cu NWs is discussed in the Supporting Information.

Analysis of Environmental Stability. The phase and purity of the as-prepared Cu NWs were examined by X-ray diffraction (XRD) (Figure 2a and Figure S4, Supporting Information). All the diffraction peaks can be indexed to face-centered cubic (*fcc*) copper with a calculated lattice constant $a = 3.617$ Å, which is in agreement with the literature value (JCPDS 4-836). A broad diffraction peak at ~20−35° is due to the glass substrate. The as-prepared Cu NWs show a good stability in the ambient environment without any specific protection. As shown in Figure 2a, their XRD patterns indicated that the sample is unchanged after storage in the dried state for more than a year. This is a surprising result. Some previous reports state that bare Cu NWs could be easily oxidized in air within a short period of time.[18,20,34]

As we discussed above, the surface of Cu NWs is adsorbed by a thin layer of protonized ODA^+ during the reaction process. Protonized ODA^+ can act as efficient corrosion inhibitor for copper because it contains an N heteroatom.[38] Wiley and co-workers also reported that Cu NWs fabricated by reducing $Cu(NO_3)_2$ with hydrazine in a solution containing ethylenediamine can remain stable in air for over one month.[39] The reason might be that the Cu NWs are bound with ethylenediamine moleculars which contain N atoms. In this case, the factors involved in the environmental stability mechanism could be possibly due to interaction of ODA^+ molecules with the surface of Cu NWs and forming strong N−Cu chemical bonds.[38] The ODA^+ molecule−surface and the lateral molecule−molecule interaction form a protective film which blocks the reactive species from close contact with the surface of Cu NWs. In order to verify the hypothesis, X-ray absorption fine structure (XAFS, including XANES and EXAFS) spectroscopy, a method for the identification of the local environment around a specific atom,[40] was conducted to confirm the formation of N−Cu bonds at the interface between Cu NW and adsorbate layer. Figure 2b shows the normalized XAFS spectra of Cu foil and Cu NW sample. The XAFS profile of the Cu NWs demonstrates a very close resemblance to that of the Cu foil, indicating the high stability of the Cu NWs. Only the intensity of oscillation is smaller than Cu foil, which is a typical signature of nano-Cu compared to bulk Cu.[41] The electronic and geometric structural information on the Cu NWs could be further unraveled in Figure 2c and d. There is a shift to higher energy for Cu NW sample compared to bulk Cu foil (see Figure 2c), illustrating that there is chemical reactions between Cu nanowire surface and other elements. The Fourier transforms (FT) of the EXAFS spectra of the Cu foil and Cu NWs shown in Figure 2d demonstrate a strong Cu−Cu peak located at 2.52 Å.[42] While for the Cu NWs, the new peak at around 1.42 Å might be ascribed to the formation of Cu−N bonds at the Cu nanowire surface.[42,43] The presence of N−Cu bonds on the surface of Cu NWs would greatly restrain the oxidation process.

Construction of Individual Cu Nanowire-Based Nanodevices. The nanodevices based on individual Cu NW were fabricated on SiO_2/Si substrate (SiO_2 layer with a thickness of 500 nm) with predeposited Au/Ti microelectrodes (Figure 3a). An individual Cu NW was first transferred among the microelectrodes and was then connected to Pt microleads by FIB deposition. This technique warrants ohmic contacts and allows the intrinsic electrical properties of NWs to be measured.[44−47] To examine the intrinsic electrical properties of individual Cu NW, the four-probe method is suitable because

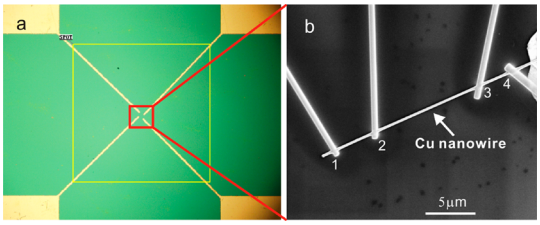

Figure 3. (a) Optical micrograph of Au/Ti microelectrode pattern on SiO_2/Si layer. The distance between each microelectrode is 10 μm. (b) Typical SEM image of a nanodevice based on individual Cu NW (diameter ~250 nm) with four-terminal configuration (see text for details).

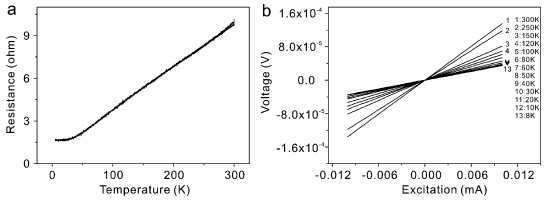

Figure 4. (a) Temperature dependence of the resistance of an individual Cu NW. The resistance was measured by the four-probe method in the temperature range of 5−300 K. (b) $I-V$ curves of the Cu NW device measured at a series of temperature in the range of 300 to 8 K.

it can eliminate the influence of the contact resistance.[44,47] Figure 3b shows a typical SEM image of the nanodevice based on individual Cu NW with four-terminal configuration, first etching a small square piece of outer layer about 5 nm in depth by FIB (at positions 1, 2, 3, and 4, respectively), then Pt microleads were directly deposited on the Cu NW and connected to Au/Ti microelectrodes (Figure 3b). Three segments of the device have different lengths of $L_{12} = 4.53$ μm, $L_{23} = 11.56$ μm, and $L_{34} = 3.91$ μm (see Figure 3b).

Electrical Property. The electrical properties were measured by the four-probe method within a physical property measurement system (PPMs). Figure 4a shows the temperature dependence of the resistance of a typical individual Cu NW (Figure 3b). The Pt microleads 1−4 are denoted as I^+, V^+, V^-, I^-, respectively. A small constant current (300 nA) is fed between Pt microleads 1 and 4. Meanwhile, a potential drop is acquired between Pt microleads 2 and 3 in the temperature range of 5−300 K. Due to the fact that the PPMs cannot stably reach the temperature below 5 K, the electrical behavior of the Cu NW below this temperature is still unknown. Thus, the intrinsic electrical resistance between Pt microleads 2 and 3 can be measured in the temperature range of 5−300 K, as shown in Figure 4a. Clearly, the resistance data are typical of a good metal. The resistance (R) versus temperature (T) curve displays a fairly linear $R-T$ behavior from 300 K to about 25 K and reaches a residual resistance below 25 K with a residual resistivity ratio $\rho_{300K}/\rho_{5K} \sim 6$. The resistance does not show any upturn at low temperature, thus ruling out any significant disorder in the NW that can give rise to effects such as localization, in agreement with the electrical behavior of Cu@C nanocables.[35] Because Cu NW is a nonmagnetic metallic crystalline solid, the temperature dependence of the electrical resistance arises mainly from the electron−phonon interaction.[48] By comparison, Lu and co-workers reported that electrical resistivity of Cu sample with nanoscale twins and coarse-grained Cu decreases linearly with the temperature down to about 70 K because of the dominant scattering of grain boundaries below 70 K.[49] Therefore, our experiment results further confirm well-crystallized structure of the Cu NW of this case.

Figure 4b shows the $I-V$ curves of the Cu NW device (Figure 3b) measured at a series of temperatures in the range of 300 to 8 K. All the $I-V$ curves at different temperature exhibit a perfect linear dependence, thus demonstrating ohmic behavior,[8,50] which illustrates that $R-T$ behavior shown in Figure 4a reflects the intrinsic electrical characteristic of the Cu NW and the value of the slop of $I-V$ curves at different temperatures is consistent with that of the $R-T$ curve. At room temperature (300 K), the resistance of the Cu NW is about 9.895 Ω (R_{300K}) from the $R-T$ curve (Figure 4a). The resistivity of the Cu NW, ρ_{300K}, could be extracted from the formula: $R_{300K} - Rc \approx \rho_{300K}L/A$, since Ohm's law remains valid in the nanoscale regime.[51] Rc represents the temperature-independent part of the resistance, including surface scattering and contact resistance, and in this case $Rc \approx R_{5K}$ (≈ 1.64 Ω from Figure 4a) because the resistance of Cu NWs was reported to reach a residual value at $T = 4.2$ K.[52] L is L_{23} (11.56 μm; see SEM image shown in Figure 3b), and A is the cross-sectional area of the Cu NW (the diameter of the Cu NW: ~ 250 nm from SEM image in Figure 3b, $A = \pi$ (250/2)^2 nm^2). The resistivity ρ_{300K} is calculated as about 3.5×10^{-6} Ω·cm, which is similar to the resistivity of Cu NW core inside an amorhous carbon sheath(2.65×10^{-6} Ω·cm),[35] and the resistivity of a single 400 nm diameter highly twinned Cu NW (1.84×10^{-6} Ω·cm).[17] The results demonstrate that this kind of individual Cu NW can retain the excellent electrical property. Meanwhile, the maximum transport current density (J_{max}) for the individual Cu NW was determined by performing on the NW of the middle part of the nanodevice in Figure 3b by using two-probe measurements inside a SEM system equipped with a Zyvex S100 nanomanipulator. A Keithley 4200 source meter was used for the electrical measurements.

Figure 5a shows a typical SEM image of the individual Cu NW device of Figure 3b at low magnification. The individual Cu NW was connected to four Au/Ti microelectrodes by ion-beam-induced deposition of Pt. The maximum transport current density was measured by performing on the Cu NW between Pt microleads 2 and 3 using two-probe measurement. The arrows show the testing current direction. Figure 5b shows the corresponding SEM image of this device

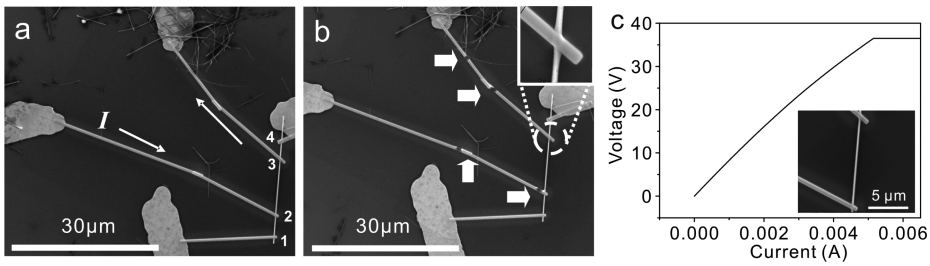

Figure 5. (a) SEM image of the individual Cu NW device of Figure 3b at low magnification. The individual Cu NW was connected to four Au/Ti microelectrodes by ion-beam-induced deposition of Pt. The maximum transport current density was measured by performing on the Cu NW between Pt microleads 2 and 3 using two-probe measurement. The arrows show the testing current direction. (b) SEM image of the Cu NW device shown in (a) after testing for the maximum current it could support. The failure point is indicated by arrows. The inset (top right) is the zoom-in of the SEM image of the indicated part. (c) *I*−*V* curve recorded for the Cu NW device shown in (a) that broke down at a current of about 5.2 mA at room temperature. The inset is the corresponding SEM image of this device being tested.

after testing for the maximum current it could support. Figure 5c shows that the Cu NW could endure a current of up to 5.2 mA before failure, which corresponds to a current density of 1.06×10^7 A·cm^{-2}. To our surprise, the failure points occurred at several places of Pt microleads, instead of the Cu NW, as indicated by arrows in the SEM image in Figure 5b. As shown in the inset of Figure 5b, the diameter of the Pt microlead is about 600 nm, while that of the Cu NW is 250 nm. But the Cu NW shows stronger than Pt microleads. The reason might be explained as follows: The Pt microleads deposited by FIB are polycrystalline,[24] containing many crystal grains. Electron scattering occurs preferentially at crystal grain boundaries,[8] which generates high resistive self-heating, resulting in low failure current densities. As for the Cu NW, with its single crystalline nature, it is free of energy dissipation and void diffusion at the grain boundary or defect sites, giving high failure current densities.[8] So the maximum transport current density for the Cu NW should be superior to 1.06×10^7 A·cm^{-2}, similar to the breakdown current density of individual Cu@C nanocable (5.78×10^7 A·cm^{-2}) and 740 nm-diameter Cu wire made by meniscus-confined 3D electrodeposition (1.25×10^7 A·cm^{-2}).[2,35]

In addition, the as-prepared Cu NWs have ultralow junction resistance besides environmental stability and superb electrical properties, which are different from Cu@C nanocables (the outer amorphous carbon layer is isolating, preventing Cu@C nanocables from being interconnecting).[35] To evaluate the effect of NW−NW junction resistance, the electrical transport properties of the Cu NW networks with a thickness of about 2 μm were measured within PPMs by using a four-probe method. Figure S5 (Supporting Information) shows the temperature dependence of the surface resistance of the Cu NW networks measured in the temperature range of 5−300 K. Clearly, *R*−*T* curves are smooth, and the surface resistance decreases with the decreasing temperature, indicating a good metal character of the Cu NW networks. At room temperature, the surface resistance of the Cu NW network was measured to be 0.63 Ω/sq, indicating good electrical transport property of the Cu NW networks and inferring ultralow NW−NW junction resistance. This attractive characteristic can make the Cu NWs for use as multifunctional building blocks in future nanodvices, such as the need for direct communication between cross interconnects, and for use as transparent electrodes to be a replacement for indium tin oxide films.[39,53,54]

Mechanical Property. To qualitatively determine the mechanical strength, mechanical tests on individual Cu NWs with different diameters were performed inside a SEM system equipped with a Zyvex S100 nanomanipulator, as shown in Figure 6. An individual Cu NW was positioned lying on a silicon wafer with patterns of tunnel arrays with 5 μm width and 4 μm depth. An individual Cu NW was horizontally pushed using a tungsten probe driven by the movable piezoelectric head of the holder. Figure 6a−c show a chronological series of SEM images of an individual Cu NW with a diameter of about 100 nm being horizontally pushed by a tungsten probe in before, during and after contact states, respectively. The arrows indicate the tungsten probe moving direction. We clearly see that the 100 nm diameter Cu NW bend a little first (Figure 6b) and then suddenly fracture (Figure 6c) under the applied force of the tungsten probe, indicating that the adhesion forces between the nanowire and the substrate are stronger than the mechanical strength of the nanowire to prevent the wire from moving. No residual plastic deformation or significant elongation is observed when the NW is broken, as shown in Figure 6c, demonstrating the brittle and elastic behavior of the Cu NW, which is consistent with the mechanical properties of nancrystalline Cu, and twinned Cu NWs.[17,49] Figure 6d−f show the process of a tungsten probe horizontally pushing an individual Cu NW with a diameter of about 300 nm. As seen in Figure 6e, the 300 nm diameter Cu NW gets bent as observed previously in Figure 6b and begins to move along the direction of the tungsten probe pushing (Figure 6f), indicating that the tensile strength of the Cu NW is strong enough to overcome the adhesion forces

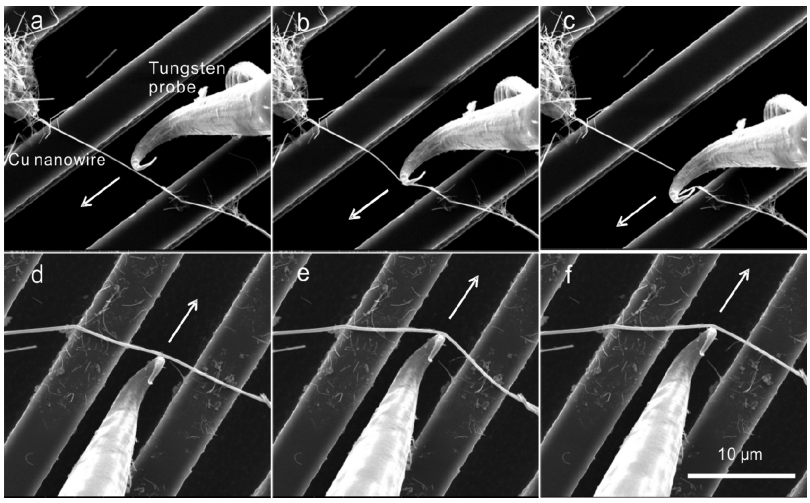

Figure 6. (a–c) A chronological series of SEM images of an individual Cu NW with a diameter of about 100 nm being horizontally pushed by a tungsten probe in before, during, and after contact states, respectively. (d–f) Horizontally pushing an individual Cu NW with a diameter of about 300 nm by a tungsten probe repeating the process from a to c. The arrows indicate the tungsten probe moving direction.

between the nanowire and the substrate. When the NW is relaxed, the plastic deformation remains because of the emergence of dislocations, indicating that large size Cu NW can tolerate dislocations while the small size NW cannot. Mechanical tests of all the NWs at different diameters were conducted following the same procedure mentioned above, and most of the Cu NWs with a diameter of 300 nm below are more susceptible to breakage. The results demonstrate that the mechanical strength of the Cu NWs decreases with decreasing diameter, which is consistent with Co NW,[5] Au NW,[55] Ge NW,[56] and Si NW.[57]

A simple experiment was designed to treat the as-prepared Cu NWs using ultrasonic cleaning to verify the size-dependence of the mechanical strength. As shown in Figure S7 (Supporting Information), we clearly see that after ultrasonic treatment the Cu NWs with large diameter remain intact. The Cu NWs with small diameters are broken, and the smaller ones become shorter. Furthermore, the mechanical properties of the as-prepared Cu NW networks were evaluated through a nanoindentation test on a Tribo Nanoindenter with a Berkovich diamond indenter. Figure S6 (Supporting Information) shows a representative nanoindentation load–displacement curve. The loading course at the beginning and the elastic response course during unloading are almost identical, indicating the absolute elastic surface of the Cu NW networks, most of which consists of Cu NWs with a diameter of 50–120 nm. An array of indentations at different indentation loads was made. The hardness value of the Cu NW networks is measured to be 35.9–96.3 MPa, far infeior to Cu film made by dc magnetron sputtering.[58] One of the reasons might be owing to the loose and rough surface of the Cu NW networks (see the inset of Figure S6, Supporting Information). Another reason might be the softening trend of Cu NWs with decreasing size, similar to Si NW and Ge NW.[56,57]

Finally, *in situ* bending measurements were carried out to quantitatively assess the response of individual Cu NWs to external loading. Individual Cu NWs were half-suspended at the edge of a silicon wafer with one end of the NWs fixed *via* an electron-beam-induced platinum deposition technique (see Figure 7).[59,60] Measurements were performed inside a SEM system and composed of visually controllable gradual bending of individual half-suspended NWs by a silicon cantilever as a force measurement system (FMS, Kleindiek, Germany). Figure 7a–d shows the snapshots of single Cu NW with a diameter of 80 nm and length of 10.55 μm during bending, as recorded in sequence under SEM. It is found that the Cu NW displays different bending states as a function of the external force. Initially, the NW is straight (Figure 7a). Subsequently, the NW undertakes a series of compression manipulations with the head of the silicon cantilever. The NW begins to bend when a pushing force is applied. Driven by the enhanced force, the NW is bent further, and the bending radius of curvature decreases gradually (Figure 7b and c). The maximum load the NW can be taken reaches 0.18 μN, and the curvature radius arrives at 1.86 μm. Mechanical stress σ in the bent NW can be calculated according to the relation $\sigma = Erk$,[61,62] where E is Young's modulus (106 GPa for Cu NW[63]), r is the radius of the Cu NW, and k is the bending curvature. The stress in the Cu NW can exceed 2.29 GPa without visible fracture. The value of the stress that the NW can endure shows the bending ability of the Cu NW. The bent NW can restore to its initial straight shape after removal of the external force, indicating the elasticity characteristic of the Cu NW. Parts e–h of Figure 7 show another bending experiment under similar conditions on a single Cu NW with a diameter of 300 nm and

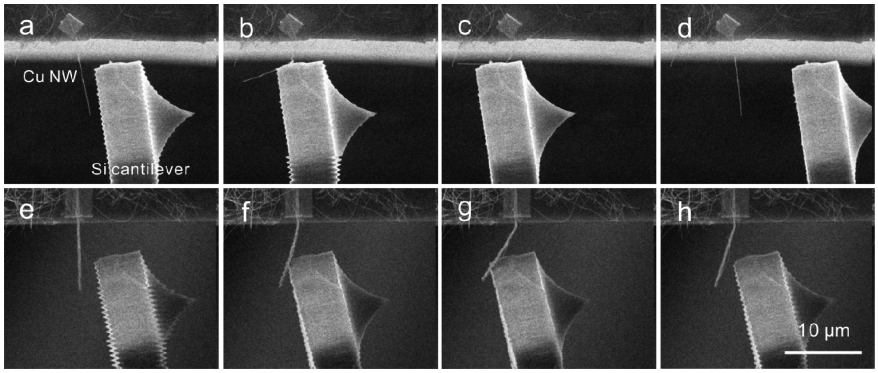

Figure 7. Consecutive SEM images of an individual Cu NW with a diameter of about 80 nm (a−d) and 300 nm (e−h), respectively, during different bending stages.

length of 9.42 μm. The Cu NW can bear the maximum load of 0.85 μN, and the curvature radius reaches 5.37 μm. The stress in the Cu NW can be estimated to be 3.02 GPa. The effect of restoration is also observed after removal of the external force, however, the initial straight profile is not reached because of residual plastic deformation.[62] In order to get deeper insight into the mechanical performance of individual Cu NWs, in total, 12 Cu NWs with different diameters were investigated, and the detailed mechanical parameters of individual Cu NWs under bending can be found in Table S1 (see the Supporting Information). From Table S1 (Supporting Information), it is concluded that the mechanical strength of Cu NWs decrease with the decreasing diameters and the small size Cu NWs tend to be elastic while the large size NWs show some extent ductility, in agreement with the experiments above. Additionally, bending experiments were performed in the same procedure on individual Cu@C nanocables reported previously,[35] in contrast to the as-prepared Cu NWs (see Figure S8, Supporting Information). From Figure S8 (Supporting Information), the single Cu@C nanocable with a diameter of 250 nm and length of 38 μm can undertake the maximum load of 0.53 μN, and the stress is estimated to be 2.12 GPa with curvature radius of 6.18 μm. The bending test shows its elasticity characteristic. While the 460 nm-diameter, 25 μm-length Cu@C nanocable can endure the maximum load of 3.76 μN, and the stress is about 3.66 GPa with curvature radius of 6.56 μm. The thicker Cu@C nanocable exhibits plastic deformation. The results of more experiments on other Cu@C nanocables indicate that the mechanical behavior of Cu@C nanocables is similar to Cu NWs. The nominal strength required in traditional wire bonding is only 8.5 MPa,[2] so the as-prepared Cu NWs are suitable for interconnects in future nanoelectronic chips.

CONCLUSIONS

In summary, ultralong individual Cu nanowire-based nanoscale devices have been constructed by using the FIB technique. $R-T$ and $I-V$ curves of individual Cu NW are measured by using the four-probe method in the temperature range of 5−300 K and typically indicate good metal character. The room-temperature resistivity of the individual Cu NW is found to be about 3.5×10^{-6} $\Omega\cdot$cm, in the same order as that of bulk copper. The maximum transport current density for the Cu NW should be superior to 1.06×10^{7} A$\cdot$cm^{-2}, and the Cu NWs have ultralow junction resistance. The mechanical tests based on individual NWs indicate that the mechanical strength decreases with the decreasing diameters, and the small-size Cu NWs tend to be brittle and elastic while the large-size NWs show some extent ductility. The present study indicates that the Cu NWs could act as ideal nanoscale building blocks for interconnects in future nanoscale devices. Furthermore, the Cu NWs could be extended to application as transparent electrodes to be a replacement for indium tin oxide films.

METHODS

Materials. ODA was purchased from Sigma-Aldrich. Other chemicals were purchased from Shanghai Chemical Reagent Co. Ltd. All chemicals were used in this study without further purification.

Synthesis of Cu NWs. The synthesis of Cu NWs was based on a modified hydrothermal method as reported previously.[19] Typically, 0.5 mmol ODA was added to 20 mL of copper(II) chloride (12.5 mmol/L) aqueous solution and vigorously stirred for 5h forming a blue emulsion. The solution was transferred into a Teflon-lined autoclave of 20 mL capacity and heated at 180 °C for 24 h. After the autoclave was cooled down to room temperature naturally, the supernatant was decanted and the red textile-like precipitate was obtained after washing with deionized water and ethanol, respectively.

Characterization. The obtained samples were characterized on an (Philips X'Pert Pro Super) X-ray powder diffractometer with Cu Ka radiation (λ = 1.541874 Å). The Cu NW sample for XRD was prepared by using a clean microscope glass slide to collect Cu NWs. The morphology was examined with a Quanta 200 FEG scanning electron microscope (SEM), a transmission electron microscope (TEM) performed on a high-resolution transmission electron microscope (HRTEM) (JEOL JEM-ARM200F)

operated at an acceleration voltage of 200 kV. Fourier transformation infrared spectroscopy (FTIR) was obtained on a Nicolet-is10 Fourier transform IR spectrometer from 4000 to 400 cm^{-1} at room temperature. The thickness of the Cu NW networks were measured using a CH-1-ST pachymeter (Shanghai Liuling Instrument Factory, China).

XAFS Measurement and Data Analysis. The Cu *K*-edge XAFS spectroscopy was recorded in the fluorescence mode at BL14W1 beamline of the Shanghai Synchrotron Radiation Facility (SSRF) using a 32-element array of Ge detectors. The acquired extended X-ray absorption fine structure (EXAFS) data were processed according to the standard procedures using the ATHENA module implemented in the IFEFFIT software packages. The EXAFS $\chi(k)$ spectra were obtained by subtracting the post edge background from the overall absorption and then normalized with respect to the edge-jump step. Subsequently, k^3-weighted $\chi(k)$ data in the *k*-space ranging from 0 to 12 $Å^{-1}$ were Fourier transformed to radial structure functions (RSF) using a hanning windows (dk = 1.0 $Å^{-1}$) to separate the EXAFS contributions from different coordination shells.

Measurements of Electrical Properties. To measure the electrical properties of a single 1D Cu NW, the as-prepared Cu NWs were first ultrasonically dispersed in anhydrous ethanol, and then a drop of the anhydrous ethanol dispersions was dried onto a silicon wafer covered with a thermally grown SiO_2 layer of 500 nm, on which Au/Ti electrode arrays were fabricated by photolithography previously (see Figure 3a). An isolated Cu NW was selected and located in a focused ion-beam (FIB) system with SEM capability (Dual-Beam 235 FIB system from FEI Co.). Platinum microleads were deposited on the isolated Cu NW by using a 30 KeV, 30 pA Ga^+ FIB, connecting to the Au/Ti electrodes. Four-probe measurement configuration was made. Electrical connection between the electrodes and the sample holder were made by an ultrasonic wire bonder. The $R-T$ curves, and $I-V$ curves were measured within a Physical Properties Measurement System (PPMS, the Quantum Design Inc.), equipped with a He-4 cryostat. To measure the electrical properties of the Cu NW networks, a piece of Cu NW networks was first transferred onto a silicon wafer covered with a thermally grown SiO_2 layer of 500 nm. Four Pt test electrodes were attached using silver epoxy. The $R-T$ curves were measured within the Physical Properties Measurement System (PPMS, Quantum Design, Inc.), equipped with a He-4 cryostat.

Mechanical Tests. To qualitatively determine the mechanical strength of an individual Cu NW, the as-prepared Cu NWs were first ultrasonically dispersed in anhydrous ethanol, and then a drop of the anhydrous ethanol dispersions was dried onto a silicon wafer, on which the patterns of tunnel arrays with 5 μm width and 4 μm depth were fabricated by photolithography previously. Then individual Cu NWs with different diameters were selected and manipulated by a tungsten probe inside a SEM system equipped with a Zyvex S100 nanomanipulator. The mechanical properties of the as-prepared Cu NW networks were evaluated through a nanoindentation test on a Tribo Nanoindenter (Hysitron Inc., Minneapolis, MN) with a Berkovich diamond indenter. The value of maximum applied force was chosen to be 10 μN to ensure that the maximum penetration depth during the tests was kept below 10% the overall film thickness. It is generally accepted that the depth of indentaition should never exceed 10% of the film thickness. Therefore, the substrate effect on the measured mechanical properties of the networks can be ignored. From the load−displacement curve, hardness can be obtained at the peak load as

$$H = \frac{P_{max}}{A}$$

where P_{max} is the peak load and A is the projected contact area.

The bending of nanowire was carried out by a silicon cantilever as a force measurement system (FMS, Kleindiek, Germany) installed in the SEM sample chamber. Half-suspended Cu NW was fixed at the edge of silicon wafer *via* an electron-beam-induced platinum deposition (Auriga, ZEISS).

Conflict of Interest: The authors declare no competing financial interest.

Acknowledgment. This research was supported by the National Basic Research Program of China (2011CB933700), the Natural Science Foundation of China (50901073 and U1432131), and the One Hundred Person Project of the Chinese Academy of Sciences, China. We are grateful to Dr. Lina Li (Shanghai Synchrotron Radiation Facility) for the help on XAFS measurement, Dr. Jun Han (Paul Scherrer Institut, Switzerland), Dr. Qingyu Kong (X-ray Science Division, Argonne National Laboratory), and Dr. Hao Cheng (National Synchrotron Radiation Laboratory, USTC) for their great help on the analysis of XAFS data and helpful discussion.

Supporting Information Available: Optical images, FTIR spectra, XRD pattern, $R-T$ curve of the Cu NW networks, and bending of Cu@C nanocables and other materials. This material is available free of charge *via* the Internet at http://pubs.acs.org.

REFERENCES AND NOTES

1. Ferry, D. K. Materials Science - Nanowires in Nanoelectronics. *Science* **2008**, *319*, 579–580.
2. Hu, J.; Yu, M. F. Meniscus-Confined Three-Dimensional Electrodeposition for Direct Writing of Wire Bonds. *Science* **2010**, *329*, 313–316.
3. Freer, E. M.; Grachev, O.; Duan, X. F.; Martin, S.; Stumbo, D. P. High-Yield Self-Limiting Single-Nanowire Assembly with Dielectrophoresis. *Nat. Nanotechnol.* **2010**, *5*, 525–530.
4. Jeong, S. J.; Moon, H. S.; Shin, J.; Kim, B. H.; Shin, D. O.; Kim, J. Y.; Lee, Y. H.; Kim, J. U.; Kim, S. O. One-Dimensional Metal Nanowire Assembly *via* Block Copolymer Soft Graphoepitaxy. *Nano Lett.* **2010**, *10*, 3500–3505.
5. Huang, X. H.; Quinto-Su, P. A.; Gonzalez-Avila, S. R.; Wu, T.; Ohl, C. D. Controlled Manipulation and *in Situ* Mechanical Measurement of Single Co Nanowire with a Laser-Induced Cavitation Bubble. *Nano Lett.* **2010**, *10*, 3846–3851.
6. Lu, Y.; Huang, J. Y.; Wang, C.; Sun, S. H.; Lou, J. Cold Welding of Ultrathin Gold Nanowires. *Nat. Nanotechnol.* **2010**, *5*, 218–224.
7. Wang, J. W.; Auyeung, R. C. Y.; Kim, H.; Charipar, N. A.; Pique, A. Three-Dimensional Printing of Interconnects by Laser Direct-Write of Silver Nanopastes. *Adv. Mater.* **2010**, *22*, 4462–4466.
8. Wang, C.; Hu, Y. J.; Lieber, C. M.; Sun, S. H. Ultrathin Au Nanowires and Their Transport Properties. *J. Am. Chem. Soc.* **2008**, *130*, 8902–8903.
9. Critchley, K.; Khanal, B. P.; Gorzny, M. L.; Vigderman, L.; Evans, S. D.; Zubarev, E. R.; Kotov, N. A. Near-Bulk Conductivity of Gold Nanowires As Nanoscale Interconnects and the Role of Atomically Smooth Interface. *Adv. Mater.* **2010**, *22*, 2338–2342.
10. Yao, Z.; Kane, C. L.; Dekker, C. High-Field Electrical Transport in Single-Wall Carbon Nanotubes. *Phys. Rev. Lett.* **2000**, *84*, 2941–2944.
11. Sun, Y. G.; Gates, B.; Mayers, B.; Xia, Y. N. Crystalline Silver Nanowires by Soft Solution Processing. *Nano Lett.* **2002**, *2*, 165–168.
12. Sun, Y. G.; Yin, Y. D.; Mayers, B. T.; Herricks, T.; Xia, Y. N. Uniform Silver Nanowires Synthesis by Reducing $AgNO_3$ with Ethylene Glycol in the Presence of Seeds and Poly-(Vinyl Pyrrolidone). *Chem. Mater.* **2002**, *14*, 4736–4745.
13. Wiley, B. J.; Wang, Z. H.; Wei, J.; Yin, Y. D.; Cobden, D. H.; Xia, Y. N. Synthesis and Electrical Characterization of Silver Nanobeams. *Nano Lett.* **2006**, *6*, 2273–2278.
14. Xu, W. H.; Yu, S. H. Conducting Performance of Individual Ag@C Coaxial Nanocables: Ideal Building Blocks for Interconnects in Nanoscale Devices. *Small* **2009**, *5*, 460–465.
15. Luo, L. B.; Yu, S. H.; Qian, H. S.; Zhou, T. Large-Scale Fabrication of Flexible Silver/Cross-Linked Poly(Vinyl Alcohol) Coaxial Nanocables by a Facile Solution Approach. *J. Am. Chem. Soc.* **2005**, *127*, 2822–2823.
16. Gao, M. R.; Xu, W. H.; Luo, L. B.; Zhan, Y. J.; Yu, S. H. Coaxial Metal Nano-/Microcables with Isolating Sheath: Synthetic Methodology and Their Application as Interconnects. *Adv. Mater.* **2010**, *22*, 1977–1981.
17. Zhong, S.; Koch, T.; Wang, M.; Scherer, T.; Walheim, S.; Hahn, H.; Schimmel, T. Nanoscale Twinned Copper

Nanowire Formation by Direct Electrodeposition. *Small* **2009**, *5*, 2265–2270.
18. Mohl, M.; Pusztai, P.; Kukovecz, A.; Konya, Z.; Kukkola, J.; Kordas, K.; Vajtai, R.; Ajayan, P. M. Low-Temperature Large-Scale Synthesis and Electrical Testing of Ultralong Copper Nanowires. *Langmuir* **2010**, *26*, 16496–16502.
19. Shi, Y.; Li, H.; Chen, L. Q.; Huang, X. J. Obtaining Ultra-Long Copper Nanowires *via* a Hydrothermal Process. *Sci. Technol. Adv. Mater.* **2005**, *6*, 761–765.
20. Toimil-Molares, M. E.; Hohberger, E. M.; Schaeflein, C.; Blick, R. H.; Neumann, R.; Trautmann, C. Electrical Characterization of Electrochemically Grown Single Copper Nanowires. *Appl. Phys. Lett.* **2003**, *82*, 2139–2141.
21. Zach, M. P.; Ng, K. H.; Penner, R. M. Molybdenum Nanowires by Electrodeposition. *Science* **2000**, *290*, 2120–2123.
22. Wang, Y. L.; Jiang, X. C.; Herricks, T.; Xia, Y. N. Single Crystalline Nanowires of Lead: Large-Scale Synthesis, Mechanistic Studies, and Transport Measurements. *J. Phys. Chem. B* **2004**, *108*, 8631–8640.
23. Wang, J.; Ma, X. C.; Qi, Y.; Ji, S. H.; Fu, Y. S.; Lu, L.; Jin, A. Z.; Gu, C. Z.; Xie, X. C.; Tian, M. L.; et al. Dissipation in an Ultrathin Superconducting Single-Crystal Pb Nanobridge. *J. Appl. Phys.* **2009**, *106*, 034301.
24. Marzi, G. D.; Iacopino, D.; Quinn, A. J.; Redmond, G. Probing Intrinsic Transport Properties of Single Metal Nanowires: Direct-Write Contact Formation Using a Focused Ion Beam. *J. Appl. Phys.* **2004**, *96*, 3458–3462.
25. Chueh, Y. L.; Hsieh, C. H.; Chang, M. T.; Chou, L. J.; Lao, C. S.; Song, J. H.; Gan, J. Y.; Wang, Z. L. RuO_2 Nanowires and RuO_2/TiO_2 Core/Shell Nanowires: From Synthesis to Mechanical, Optical, Electrical, and Photoconductive Properties. *Adv. Mater.* **2007**, *19*, 143–149.
26. Song, Y. P.; Jin, S. Synthesis and Properties of Single-Crystal Beta(3)- Ni_3Si Nanowires. *Appl. Phys. Lett.* **2007**, *90*, 173122.
27. Hassanien, R.; Al-Hinai, M.; Al-Said, S. A. F.; Little, R.; Siller, L.; Wright, N. G.; Houlton, A.; Horrocks, B. R. Preparation and Characterization of Conductive and Photoluminescent DNA-Templated Polyindole Nanowires. *ACS Nano* **2010**, *4*, 2149–2159.
28. Wang, Y.; Tran, H. D.; Liao, L.; Duan, X. F.; Kaner, R. B. Nanoscale Morphology, Dimensional Control, and Electrical Properties of Oligoanilines. *J. Am. Chem. Soc.* **2010**, *132*, 10365–10373.
29. Charlier, J. C.; Blase, X.; Roche, S. Electronic and Transport Properties of Nanotubes. *Rev. Mod. Phys.* **2007**, *79*, 677–732.
30. Avouris, P.; Chen, J. Nanotube Electronics and Optoelectronics. *Mater. Today* **2006**, *9*, 46–54.
31. Robertson, J. Growth of Nanotubes for Electronics. *Mater. Today* **2007**, *10*, 36–43.
32. Javey, A. The 2008 Kavli Prize in Nanoscience: Carbon Nanotubes. *ACS Nano* **2008**, *2*, 1329–1335.
33. Huang, Q. J.; Lilley, C. M.; Bode, M.; Divan, R. Surface and Size Effects on the Electrical Properties of Cu Nanowires. *J. Appl. Phys.* **2008**, *104*, 023709.
34. Rathmell, A. R.; Nguyen, M.; Chi, M. F.; Wiley, B. J. Synthesis of Oxidation-Resistant Cupronickel Nanowires for Transparent Conducting Nanowire Networks. *Nano Lett.* **2012**, *12*, 3193–3199.
35. Xu, W. H.; Zhang, Y. X.; Guo, Z.; Chen, X.; Liu, J. H.; Huang, X. J.; Yu, S. H. Conduction Performance of Individual Cu@C Coaxial Nanocable Connectors. *Small* **2012**, *8*, 53–58.
36. Wang, Y. B.; Wang, L. F.; Joyce, H. J.; Gao, Q.; Liao, X. Z.; Mai, Y. W.; Tan, H. H.; Zou, J.; Ringer, S. P.; Gao, H. J.; *et al.* Super Deformability and Young's Modulus of GaAs Nanowires. *Adv. Mater.* **2011**, *23*, 1356–1360.
37. Huang, J. Y.; Zheng, H.; Mao, S. X.; Li, Q. M.; Wang, G. T. *In Situ* Nanomechanics of GaN Nanowires. *Nano Lett.* **2011**, *11*, 1618–1622.
38. Kokalj, A.; Peljhan, S.; Finsgar, M.; Milosev, I. What Determines the Inhibition Effectiveness of ATA, BTAH, and BTAOH Corrosion Inhibitors on Copper? *J. Am. Chem. Soc.* **2010**, *132*, 16657–16668.
39. Rathmell, A. R.; Bergin, S. M.; Hua, Y. L.; Li, Z. Y.; Wiley, B. J. The Growth Mechanism of Copper Nanowires and Their Properties in Flexible, Transparent Conducting Films. *Adv. Mater.* **2010**, *22*, 3558–3563.
40. Liu, Q.; He, J.; Yao, T.; Sun, Z.; Cheng, W.; He, S.; Xie, Y.; Peng, Y.; Cheng, H.; Sun, Y.; *et al.* Aligned Fe_2TiO_5-Containing Nanotube Arrays with Low Onset Potential for Visible-Light Water Oxidation. *Nat. Commun.* **2014**, 10.1038/ncomms6122.
41. Jentys, A. Estimation of Mean Size and Shape of Small Metal Particles by EXAFS. *Phys. Chem. Chem. Phys.* **1999**, *1*, 4059–4063.
42. Grandjean, D.; Pelipenko, V.; Batyrev, E. D.; van den Heuvel, J. C.; Khassin, A. A.; Yurieva, T. M.; Weckhuysen, B. M. Dynamic Cu/Zn Interaction in SiO_2 Supported Methanol Synthesis Catalysts Unraveled by *in Situ* XAFS. *J. Phys. Chem. C* **2011**, *115*, 20175–20191.
43. Nishimura, S.; Takagaki, A.; Maenosono, S.; Ebitani, K. *In Situ* Time-Resolved XAFS Study on the Formation Mechanism of Cu Nanoparticles Using Poly (N-Vinyl-2-Pyrrolidone) as a Capping Agent. *Langmuir* **2010**, *26*, 4473–4479.
44. Long, Y. Z.; Zhang, L. J.; Chen, Z. J.; Huang, K.; Yang, Y. S.; Xiao, H. M.; Wan, M. X.; Jin, A. Z.; Gu, C. Z. Electronic Transport in Single Polyaniline and Polypyrrole Microtubes. *Phys. Rev. B* **2005**, *71*, 165421.
45. Chen, Z. J.; Shen, J. Y.; Wang, N. L.; Yan, H. L.; Shi, G. Q.; Jin, A. Z.; Gu, C. Z. Electrical Properties of a Single Electrochemically Template-Synthesized Polypyrrole Nanowire. *Appl. Phys. Lett.* **2006**, *88*, 253106.
46. Long, Y.; Chen, Z. J.; Wang, N. L.; Ma, Y. J.; Zhang, Z.; Zhang, L. J.; Wan, M. X. Electrical Conductivity of a Single Conducting Polyaniline Nanotube. *Appl. Phys. Lett.* **2003**, *83*, 1863–1865.
47. Tang, C. C.; Bando, Y.; Huang, Y.; Yue, S. L.; Gu, C. Z.; Xu, F. F.; Golberg, D. Fluorination and Electrical Conductivity of BN Nanotubes. *J. Am. Chem. Soc.* **2005**, *127*, 6552–6553.
48. Lee, P. A.; Ramakrishnan, T. V. Disordered Electronic Systems. *Rev. Mod. Phys.* **1985**, *57*, 287–337.
49. Lu, L.; Shen, Y. F.; Chen, X. H.; Qian, L. H.; Lu, K. Ultrahigh Strength and High Electrical Conductivity in Copper. *Science* **2004**, *304*, 422–426.
50. Tan, Y. W.; Xue, X. Y.; Peng, Q.; Zhao, H.; Wang, T. H.; Li, Y. D. Controllable Fabrication and Electrical Performance of Single Crystalline Cu_2O Nanowires with High Aspect Ratios. *Nano Lett.* **2007**, *7*, 3723–3728.
51. Weber, B.; Mahapatra, S.; Ryu, H.; Lee, S.; Fuhrer, A.; Reusch, T. C. G.; Thompson, D. L.; Lee, W. C. T.; Klimeck, G.; Hollenberg, L. C. L.; *et al.* Ohm's Law Survives to the Atomic Scale. *Science* **2012**, *335*, 64–67.
52. Bid, A.; Bora, A.; Raychaudhuri, A. K. Temperature Dependence of the Resistance of Metallic Nanowires of Diameter $\geq$ 15 nm: Applicability of Bloch-Gruneisen Theorem. *Phys. Rev. B* **2006**, *74*, 035426.
53. Wu, H.; Hu, L. B.; Rowell, M. W.; Kong, D. S.; Cha, J. J.; McDonough, J. R.; Zhu, J.; Yang, Y.; McGehee, M. D.; Cui, Y. Electrospun Metal Nanofiber Webs as High-Performance Transparent Electrode. *Nano Lett.* **2010**, *10*, 4242–4248.
54. Zhu, R.; Chung, C. H.; Cha, K. C.; Yang, W. B.; Zheng, Y. B.; Zhou, H. P.; Song, T. B.; Chen, C. C.; Weiss, P. S.; Li, G.; *et al.* Fused Silver Nanowires with Metal Oxide Nanoparticles and Organic Polymers for Highly Transparent Conductors. *ACS Nano* **2011**, *5*, 9877–9882.
55. Li, M.; Mayer, T. S.; Sioss, J. A.; Keating, C. D.; Bhiladvala, R. B. Template-Grown Metal Nanowires as Resonators: Performance and Characterization of Dissipative and Elastic Properties. *Nano Lett.* **2007**, *7*, 3281–3284.
56. Smith, D. A.; Holmberg, V. C.; Lee, D. C.; Korgel, B. A. Young's Modulus and Size-Dependent Mechanical Quality Factor of Nanoelectromechanical Germanium Nanowire Resonators. *J. Phys. Chem. C* **2008**, *112*, 10725–10729.
57. Zhu, Y.; Xu, F.; Qin, Q. Q.; Fung, W. Y.; Lu, W. Mechanical Properties of Vapor-Liquid-Solid Synthesized Silicon Nanowires. *Nano Lett.* **2009**, *9*, 3934–3939.
58. Cao, Z. H.; Li, P. Y.; Lu, H. M.; Huang, Y. L.; Meng, X. K. Thickness and Grain Size Dependent Mechanical

Properties of Cu Films Studied by Nanoindentation Tests. *J. Phys. D: Appl. Phys.* **2009**, *42*, 065405.
59. Tang, D. M.; Ren, C. L.; Wang, M. S.; Wei, X. L.; Kawamoto, N.; Liu, C.; Bando, Y.; Mitome, M.; Fukata, N.; Golberg, D. Mechanical Properties of Si Nanowires as Revealed by *in Situ* Transmission Electron Microscopy and Molecular Dynamics Simulations. *Nano Lett.* **2012**, *12*, 1898–1904.
60. Liu, F.; Tang, D. M.; Gan, H. B.; Mo, X. S.; Chen, J.; Deng, S. Z.; Xu, N. S.; Bando, Y.; Golberg, D. Individual Boron Nanowire Has Ultrahigh Specific Young's Modulus and Fracture Strength as Revealed by *in Situ* Transmission Electron Microscopy. *ACS Nano* **2013**, *7*, 10112–10120.
61. Smith, D. A.; Holmberg, V. C.; Korgel, B. A. Flexible Germanium Nanowires: Ideal Strength, Room Temperature Plasticity, and Bendable Semiconductor Fabric. *ACS Nano* **2010**, *4*, 2356–2362.
62. Vlassov, S.; Polyakov, B.; Dorogin, L. M.; Vahtrus, M.; Mets, M.; Antsov, M.; Saar, R.; Romanov, A. E.; Lohmus, A.; Lohmus, R. Shape Restoration Effect in Ag-SiO_2 Core-Shell Nanowires. *Nano Lett.* **2014**, *14*, 5201–5205.
63. Gao, Y. J.; Wang, H. B.; Zhao, J. W.; Sun, C. Q.; Wang, F. Y. Anisotropic and Temperature Effects on Mechanical Properties of Copper Nanowires under Tensile Loading. *Comput. Mater. Sci.* **2011**, *50*, 3032–3037.